Anomalous Hall conductivity and electronic structures of Si-substituted Mn_2CoAl epitaxial films

K. Arima,[1] F. Kuroda,[1] S. Yamada,[1,2] T. Fukushima,[2,3,4] T. Oguchi,[2,5,6,*] and K. Hamaya[1,2,†]

[1]*Graduate School of Engineering Science, Osaka University, Toyonaka 560-8531, Japan*
[2]*Center for Spintronics Research Network, Osaka University, Toyonaka 560-8531, Japan*
[3]*Institute for NanoScience Design, Osaka University, Toyonaka, Osaka 560-8531, Japan*
[4]*Institute for Datability Science, Osaka University, Suita, Osaka 565-0871, Japan*
[5]*Institute of Scientific and Industrial Research, Osaka University, Ibaraki, Osaka 567-0047, Japan*
[6]*MI2I, National Institute for Materials Science, Tsukuba 305-0047, Japan*

(Received 1 October 2017; published 26 February 2018)

We study anomalous Hall conductivity (σ_{AHC}) and electronic band structures of Si-substituted Mn_2CoAl ($Mn_2CoAl_{1-x}Si_x$). First-principles calculations reveal that the electronic band structure is like a spin-gapless system even after substituting a quaternary element of Si for Al up to $x = 0.2$ in $Mn_2CoAl_{1-x}Si_x$. This means that the Si substitution enables the Fermi-level shift without largely changing the electronic structures in Mn_2CoAl. By using molecular beam epitaxy techniques, $Mn_2CoAl_{1-x}Si_x$ epitaxial films can be grown, leading to the systematic control of x ($0 \leq x \leq 0.3$). In addition to the electrical conductivity, the values of σ_{AHC} for the $Mn_2CoAl_{1-x}Si_x$ films are similar to those in Mn_2CoAl films shown in previous reports. We note that a very small σ_{AHC} of ∼1.1 S/cm is obtained for $x = 0.225$, and the sign of σ_{AHC} is changed from positive to negative at around $x = 0.25$. We discuss the origin of the sign reversal of σ_{AHC} as a consequence of the Fermi-level shift in Mn_2CoAl. Considering the presence of the structural disorder in the $Mn_2CoAl_{1-x}Si_x$ films, we can conclude that the small value and sign reversal of σ_{AHC} are not related to the characteristics of spin-gapless semiconductors.

DOI: 10.1103/PhysRevB.97.054427

I. INTRODUCTION

When the conduction and valence band edges meet at the Fermi level and there is no gap for one spin channel while there is a finite gap in another spin channel, these materials are so-called spin-gapless semiconductors (SGSs) [1–3]. In the field of spintronics, because the SGSs have intriguing physical properties such as electric-field-induced magnetization changes, these materials can be utilized as ferromagnetic semiconductors [4]. Also, since not only the electrons but also the holes can become fully spin polarized [1–3], one can utilize these materials as highly efficient spin injectors and highly spin polarized channels with tunable magnetic properties.

In recent years, Ouardi *et al.* experimentally demonstrated that an inverse Heusler compound Mn_2CoAl (MCA) shows SGS characteristics such as the vanishing Seebeck coefficient and positive nonsaturating magnetoresistance with a linear change [5]. Also, the expected carrier mobility of the MCA bulk has reached ∼70 000 cm^2/V s, calculated from the results in Ref. [5]. Since the observations of these characteristics, lots of theories and experiments on SGS characteristics of Heusler compounds for both bulk and films have been reported [6–16]. For MCA films, however, there is no report on the vanishing Seebeck coefficient and/or on the positive nonsaturating magnetoresistance. Also, there is a large difference in the carrier concentration between the bulk in Ref. [5] (∼10^{17} cm^{-3}) and films (10^{21} cm^{-3} ∼ 10^{22} cm^{-3}) [12,14–16]. These imply that SGS characteristics have not been demonstrated in the MCA films.

On the other hand, a very small anomalous Hall conductivity (σ_{AHC}) has also been considered to be a characteristic of MCA [5]. With respect to the bulk MCA [5], a small σ_{AHC} of 21.8 S/cm was observed, although conventional ferromagnetic Heusler compounds showed relatively large σ_{AHC} of ∼1000 S/cm [17,18]. According to Ouardi *et al.* [5], a numerical calculation based on the Berry curvature showed a σ_{AHC} of 3 S/cm, which was regarded as a consequence of the antisymmetry of the Berry curvature for $\mathbf{k_z}$ vectors of opposite sign. First-principles calculations also revealed an extremely small σ_{AHC} of 0.16 S/cm for ideal (stoichiometric) MCA [19]. Namely, such small σ_{AHC} values due to the intrinsic anomalous Hall effect are peculiar properties of MCA.

Recently, relatively small σ_{AHC} values were shown experimentally even for MCA films [12,14–16]. Some of studies regarded such small σ_{AHC} values as an evidence for the realization of SGS-like MCA [14,16]. However, the experimentally reported σ_{AHC} values are scattered, and the relationship between the electrical conductivity (σ_{xx}) and the carrier concentration in MCA films cannot be understood simply as SGS characteristics like a bulk. So far, there has been no discussion about the correlation between σ_{AHC} and its electronic structures for MCA.

In this article, to examine the correlation between σ_{AHC} and electronic band structures in MCA, we conduct first-principles calculations of Si-substituted Mn_2CoAl ($Mn_2CoAl_{1-x}Si_x$), and experimentally measure σ_{AHC} for the films with various x ($0 \leq x \leq 0.3$). First-principles calculations reveal that the electronic band structure is like a spin-gapless (SG) system at

*oguchi@sanken.osaka-u.ac.jp
†hamaya@ee.es.osaka-u.ac.jp

 ©2018 American Physical Society

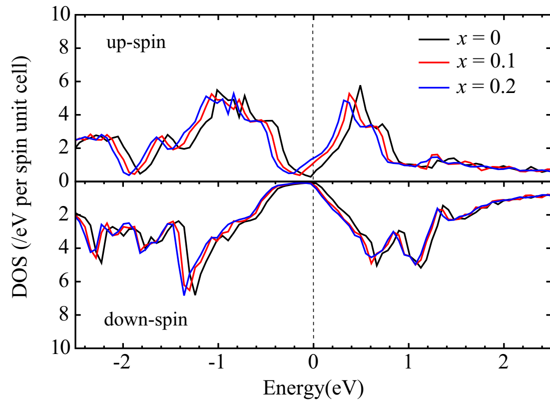

FIG. 1. Spin-resolved DOS for the Si-substituted MCA, together with the perfectly ordered MCA.

around the Fermi level even after substituting a quaternary element of Si for Al up to $x = 0.2$. This means that the Si substitution enables the Fermi-level shift without largely changing the electronic structures in MCA. By using molecular beam epitaxy (MBE) techniques, $Mn_2CoAl_{1-x}Si_x$ (MCAS) epitaxial films can be grown. In addition to the electrical conductivity, the values of σ_{AHC} for the MCAS films are similar to those in MCA films shown in previous reports. We note that a very small σ_{AHC} of $\sim$1.1 S/cm is obtained for $x = 0.225$, and the sign of σ_{AHC} is changed from positive to negative at around $x = 0.25$. We discuss the origin of the sign reversal of σ_{AHC} as a consequence of the Fermi-level shift in MCA. Because the carrier concentration of the grown MCAS films is 5 orders of magnitude larger than that of the bulk in Ref. [5], we can judge that the small value and sign reversal of σ_{AHC} are not related to the characteristics of spin-gapless semiconductors.

II. RESULTS

A. Electronic band structures

To elucidate the electronic effect of Si substitution on the electronic structure of MCA, we use the MACHIKANEYAMA 2002 program package [20], based on the Korringa-Kohn-Rostoker (KKR) Green's function method [21,22]. The shape of the crystal potential is approximated with muffin-tin potentials, and the angular momentum cutoff (l_{max}) for the Green's function is $l_{max} = 2$. We employ the generalized gradient approximation (GGA) [23] for the exchange-correlation functional. By total energy calculations, the equilibrium lattice constant of MCA is obtained to be $\sim$0.576 nm. Si substitution effects are considered within the coherent potential approximation (CPA) to treat the electronic structure and magnetism in disordered systems [24,25]. The Al sites of MCA are substituted with Si while keeping the lattice constant of pure MCA. In Fig. 1 we show the calculated spin-resolved density of states (DOS) for MCAS with $x = 0.1$ and 0.2, together with the perfectly ordered MCA ($x = 0$). Even after substituting Si for Al up to $x = 0.2$, the gapless structures in the majority-spin state can be maintained within a band gap in the minority-spin state, which are regarded as SG systems like pure MCA. When $x > 0.2$ in MCAS, a SG system-like electronic structure was broken. Thus, the Si substitution up to $x = 0.2$ can shift the position of the Fermi level for investigating σ_{AHC} in MCA systems.

B. Growth and characterizations

MCAS films ($0 \leq x \leq 0.3$) were grown on $MgAl_2O_4(100)$ substrates by MBE, where the lattice mismatch between MCA (bulk) and $MgAl_2O_4$ was $\sim$1.5%. After loading the $MgAl_2O_4(100)$ substrates into an MBE chamber, we performed a heat treatment at 600 °C for 1 hour with a base pressure of $\sim 10^{-7}$ Pa. By *in situ* reflection high-energy electron diffraction (RHEED) observations, a good surface flatness of the $MgAl_2O_4(100)$ substrate was confirmed. Cooling the substrate temperature down to 300 °C, we grew MCAS films with a thickness of $\sim$25 nm by coevaporating Mn, Co, Al, and Si using Knudsen cells. Here we used a nonstoichiometric evaporation technique [26–28] in which the evaporation ratio of Mn, Co, Al, and Si is set to 2 : 0.68 : 2.2 : x for MCAS. As an example, an *in situ* RHEED pattern for $x = 0.2$ is shown in the inset of Fig. 2(a), indicating good two-dimensional epitaxial growth of the MCAS film.

Figure 2(a) displays θ-2θ x-ray diffraction (XRD) patterns of the MCAS films for various x. For all the films, (200) and (400) diffraction peaks are clearly observed at 2θ of $\sim 31^\circ$ and 63°, respectively, indicating the formation of $B2$-ordered Heusler alloys. No diffraction peak derived from the formation of other phases is observed. The estimated lattice constant of the grown MCA ($x = 0$) was $\sim$0.587 nm, slightly larger than that of the bulk MCA ($\sim$0.579 nm) [5] and the theoretical value ($\sim$0.576 nm) in our calculations. Because half of a diagonal length of $MgAl_2O_4$ is 0.5715 nm ($1/\sqrt{2} \times$ 0.8083 nm), an in-plane lattice strain can be induced, resulting in an expansion of c-axis lattice constant for MCAS. In Fig. 2(a) we can see the slight shifts of the (200) and (400) diffraction peaks toward higher angles by increasing x, indicating that the c-axis lattice constant is gradually decreased with increasing x. This feature was consistent with the result obtained from CPA, indicating the successful substitution of Al for Si in the MCAS films.

We further characterized an MCAS film by using cross-sectional transmission electron microscopy (TEM) and energy-dispersive x-ray spectroscopy (EDX). From the TEM image in Fig. 2(b), we can recognize that the MCAS film for $x = 0.2$ is epitaxially grown on $MgAl_2O_4(100)$ with no marked defects and the surface of the MCAS film is very flat. The EDX line profiles of the MCAS/$MgAl_2O_4(100)$ heterostructure are presented in the inset of Fig. 2(b). Even though we coevaporated Mn, Co, Al, and Si with a ratio of 2 : 0.68 : 2.2 : 0.2 for the growth of MCAS ($x = 0.2$), the chemical composition of the MCAS layer along the vertical direction is nearly stoichiometric (Mn : Co : Al : Si = 2 : 1 : 0.8 : 0.2). These features are almost the same as our previous works [27,28]. For these reasons, the nonstoichiometric MBE technique used here enables us to systematically grow MCAS films on $MgAl_2O_4(100)$ with a very flat surface.

To measure electrical and magnetotransport properties, the MCAS films were patterned into Hall-bar devices $80 \times 80\ \mu m^2$ in size, as shown in the inset of Fig. 2(c), by a conventional photolithography and Ar ion-milling technique. Electrical conductivity (σ_{xx}) was measured by a standard dc four-terminal method. Figure 2(c) shows σ_{xx} as a function of

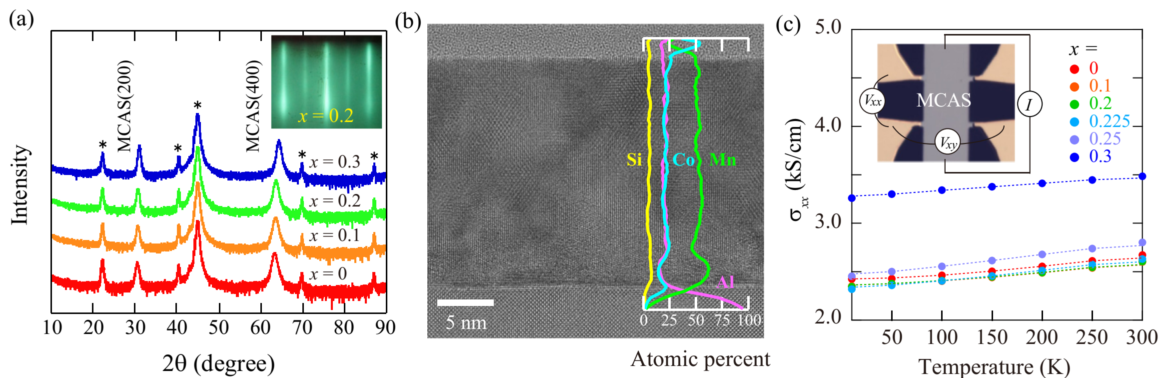

FIG. 2. (a) θ-2θ XRD patterns of the $Mn_2CoAl_{1-x}Si_x$ films. The asterisk marks correspond to the diffraction peaks derived from the $MgAl_2O_4(100)$ substrate. The inset shows a RHEED pattern of the surface for $x = 0.2$ during the growth. (b) Cross-sectional TEM image of the $Mn_2CoAl_{0.8}Si_{0.2}$ film, together with the depth profile of the atomic compositions of Mn, Co, Al, and Si. (c) Temperature dependence of σ_{xx} for various $Mn_2CoAl_{1-x}Si_x$ films. The inset shows a fabricated Hall-bar device for transport measurements.

the external temperature for various x ($0 \leq x \leq 0.3$). A weak temperature dependence with a slight positive slope of σ_{xx} (semiconducting type), almost equivalent to the bulk MCA reported previously [5], is observed for all the x. However, the value of σ_{xx} for $x = 0.3$ is relatively large compared to those for other x. A possible reason for the difference in σ_{xx} is the difference in the film quality. A detailed discussion is presented later. According to some theoretical calculations [29,30], it has been revealed that $L2_1$-type (Mn-Co-Mn-Al) MCA is a ferromagnetic metal, while XA-type (Mn_1-Mn_2-Co-Al) MCA shows a SGS. From the results of Fig. 2(c), we can tentatively judge that the predominant structure of the grown MCA and MCAS films is the XA-type structure. In particular, the σ_{xx} value for $x = 0.2$ and 0.225 at 10 K was ~2340 S/cm, which is almost equivalent to that for the bulk MCA (~2250 S/cm at 10 K) [5].

C. Magnetic properties

Magnetization curves of the various MCAS films (5 mm × 3 mm) were measured by applying in-plane magnetic fields (H). Here we used a vibrating sample magnetometer in a physical property measurement system (Quantum Design). Figure 3(a) shows the plot of the magnetic moment (M) versus H at 10 K. Because of the epitaxially grown films, there are some influences of the magnetocrystalline anisotropy on the magnetization curves in low-field regions. For all the films, the magnetic moments are saturated above 55 kOe, meaning that we can discuss the anomalous Hall effect above 55 kOe. The total magnetic moment at 10 K for all the films is nearly equivalent to that of bulk MCA reported previously [5]. However, the theoretical magnetic moment, obtained from CPA, was slightly increased by increasing x in MCAS. Also, the magnetic moments at 300 K for all the films are largely decreased compared to the bulk, as shown in the inset of Fig. 3(a). This means that the Curie temperature of the film samples is lower than that of bulk [14]. From these magnetic properties, we should consider the presence of the structural disorder in the MCAS films because of the low-temperature growth (300 °C). The influence of the presence of the disorder is discussed in the last section.

D. Anomalous Hall effect

Here we explore the anomalous Hall effect of the grown MCAS films. Figure 3(b) shows the field-dependent Hall resistivity (ρ_{xy}) at 10 K for various MCAS films ($0 \leq x \leq 0.3$). All the films evidently show the anomalous Hall effect in addition to the ordinary Hall effect in high magnetic fields, and the feature is systematically changed with increasing x. To evaluate ρ_{xy}, we used a method for the extrapolation of the $\rho_{xy} - H$ curve above 55 kOe towards zero field, as shown in the inset of Fig. 3(c). From the relation $\sigma_{yx} \approx \rho_{xy}/\rho_{xx}^2$ [31], we can estimate σ_{AHC} as the value of σ_{yx} at zero field for various x, as shown in Fig. 3(c). For $x = 0$ (MCA), a relatively small σ_{AHC} of ~8.9 S/cm is obtained, comparable to that for thin-film samples reported elsewhere [12,14–16]. Thus, we can consider that the electronic band structure of the grown MCA film is similar to that expected from a numerical calculation of σ_{AHC} based on the Berry curvature [5] or first-principles calculations [19]. With increasing x, σ_{AHC} is gradually decreased and a very small σ_{AHC} of ~1.1 S/cm is obtained for $x = 0.225$. We note that a sign reversal of σ_{AHC} from positive to negative can be seen at around $x = 0.25$. For $x = 0.3$, the magnitude of negative σ_{AHC} is further increased. These systematic changes and sign reversal of σ_{AHC} have not been seen yet in MCA systems.

III. DISCUSSION

A. An origin of the AHC sign reversal

From a theoretical point of view, we discuss an origin of the sign reversal of σ_{AHC}, shown in Fig. 3, in the MCAS films. To calculate σ_{AHC}, the QUANTUM ESPRESSO package [32] is used with the relativistic version of the ultrasoft pseudopotentials using the GGA exchange-correlation functional [23]. The wave vector **k**-point mesh is taken to be 18 × 18 × 18, and Methfessel-Paxton smearing with a broadening parameter of 0.001 Ry is used. The cutoff energy for the wave function is set to 50 Ry. The Wannier interpolation models are obtained from the first-principles band structure using the WANNIER90 program code [33]. For Mn and Co, s, p, and d orbitals are adopted to construct the Wannier function. Figure 4(a) displays the calculated electronic band structure of the MCA with a

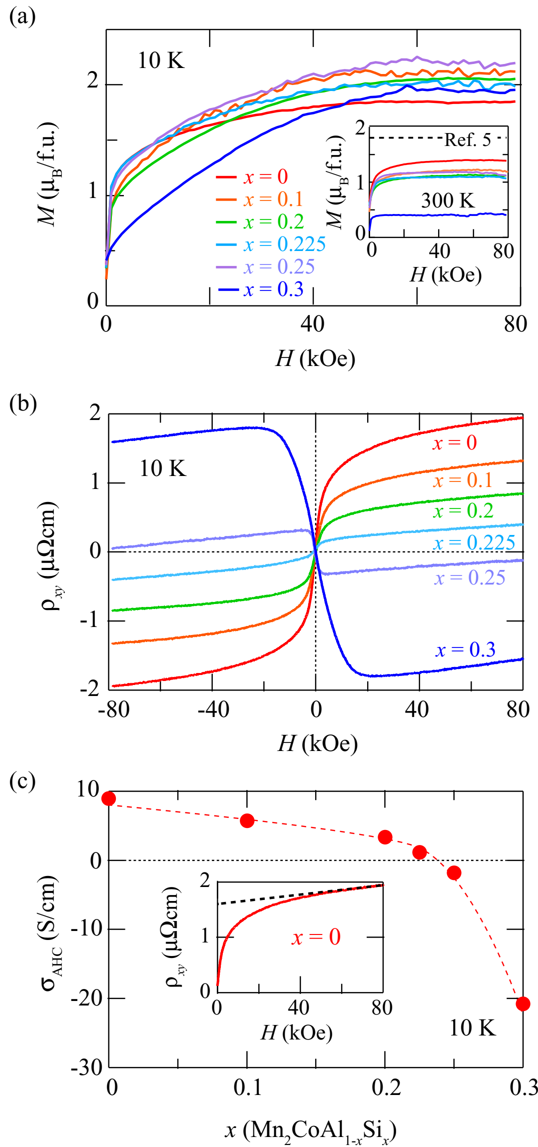

FIG. 3. (a) Field-dependent magnetic moment (M) and (b) field-dependent Hall resistivity (ρ_{xy}) at 10 K for various MCAS films. The inset of (a) shows M-H curves at 300 K. The dashed line is the value of M for the bulk sample in Ref. [5]. (c) σ_{AHC} as a function of x at 10 K. The inset shows a method for the extrapolation of the value of ρ_{xy} above 55 kOe towards zero field.

lattice constant of 0.584 nm, where this value is one of the lattice constant values for a Si-substituted MCA film ($x = 0.2$) obtained experimentally. We can confirm that the electronic band structure is similar to that of MCA reported in previous works [9,34]. The obtained Wannier interpolation energy band structure reproduces well the first-principles one as shown in the black dotted curve in Fig. 4(a). σ_{AHC} can be calculated using the Wannier interpolation models with the following equation [35–37],

$$\sigma_{AHC} = \frac{e^2}{\hbar}\int \frac{d^3\mathbf{k}}{(2\pi)^3}\Omega_z(\mathbf{k}), \tag{1}$$

where $\Omega_z(\mathbf{k})$ is the z component of the total Berry curvature for $\mathbf{k}$. Figure 4(b) shows the calculated result of σ_{AHC} versus the

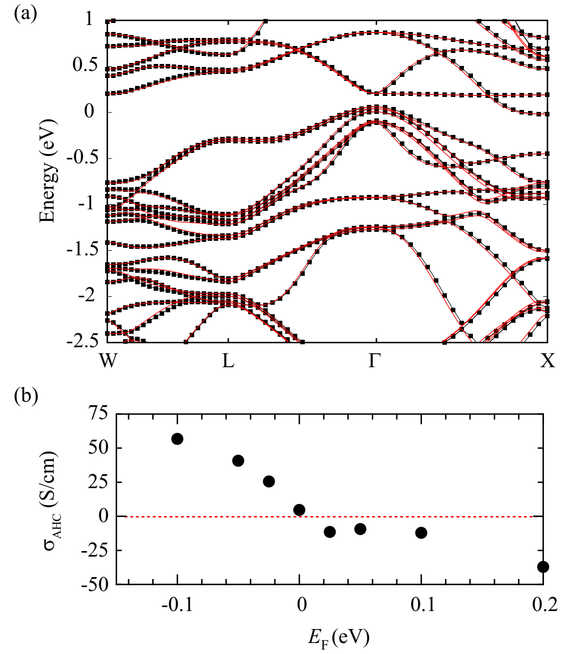

FIG. 4. (a) Electronic band structure of MCA. Black dotted and red solid curves are the energy bands obtained from first-principles calculations and Wannier interpolation, respectively. (b) The plot of σ_{AHC}, calculated from the Berry-phase approach, versus the Fermi energy.

Fermi energy (E_F). Here the lattice constant is also assumed to be 0.584 nm, taken from our experimental result for $x = 0.2$. At $E_F = 0$ (MCA), a σ_{AHC} of ~4.6 S/cm is obtained theoretically. We note that the value of σ_{AHC} can be varied with shifting the position of E_F, and the negative σ_{AHC} can be seen. In addition, from the results with virtual crystal approximation, the sign reversal of σ_{AHC} was confirmed in the Si-substituted MCA. From these considerations, the Fermi-level shift induced by the Si substitution in MCA enables the sign reversal of the σ_{AHC} value. Thus, the observed sign reversal of σ_{AHC}, shown in Fig. 3, can roughly be interpreted in terms of the energy shift of the Fermi level in the Si-substituted MCA systems.

B. Influence of Mn-Al antisite defects

From the slope of the ordinary Hall effect above 55 kOe, the carrier (hole) concentration of our MCAS films can be estimated to be $\sim 10^{22}$ cm^{-3}. This value is 5 orders of magnitude larger than that in bulk MCA ($\sim 10^{17}$ cm^{-3}) [5]. Although the value and temperature dependence of σ_{xx} for the MCAS films showed the semiconducting characteristics derived from the XA-type structure (Mn_1-Mn_2-Co-Al), we should consider the presence of the structural disorder causing a large number of additional carriers in the films. In a previous work on MCA [9], it was predicted that the SGS behavior cannot be conserved when there are antisite defects between Mn_2 and Al induced by the lattice strain, etc. At least, since the grown MCAS films are structurally affected by the lattice strain from the $MgAl_2O_4$ substrate and by the low-temperature growth, we should check the influence of the antisite defects even in MCAS. In Fig. 5

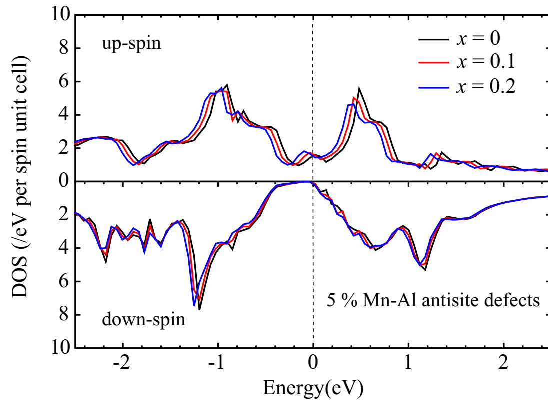

FIG. 5. Spin-resolved DOS for MCAS ($x = 0$, 0.1, and 0.2) with 5% Mn_2-Al antisite defects.

we show the influence of the Mn_2-Al antisite defects on the spin-resolved DOS of MCAS with $x = 0$, 0.1, and 0.2 using the KKR-CPA calculation, where we intentionally introduce 5% Mn_2-Al antisite defects. Unlike Fig. 1, the SGS-like electronic band structure is broken due to the formation of the majority-spin band structure at around the Fermi level, giving rise to the half-metal-like one. We infer that this majority-spin state can create a large number of carriers (holes), resulting in the unexpectedly large carrier concentration of $\sim 10^{22}$ cm^{-3}. Because the expected sign reversal of σ_{AHC} in Fig. 4(b) was governed by the relatively large Fermi-level shift in MCA, the influence of a small amount of the antisite defects on the sign reversal of σ_{AHC} might be small.

We also measured the magnetoresistance ($\rho_{xx} - H$) curve at 10 K. All the films showed negative magnetoresistance, being different from that reported in bulk MCA as mentioned in Sec. I [5]. The conventional negative magnetoresistance indicates that we have not obtained the SGS-like electronic band structure yet [38]. Furthermore, the reported magnetic properties in Sec. II C involved the presence of the disorder in MCAS films. For improving these issues, we should suppress such antisite defects and demonstrate realistic SGS electronic band structure, even in the film samples.

IV. CONCLUSION

We have studied σ_{AHC} and electronic band structures of Si-substituted Mn_2CoAl ($Mn_2CoAl_{1-x}Si_x$). First-principles calculations revealed that the electronic band structure is like a SG system even after substituting a quaternary element of Si for Al up to $x = 0.2$. Using molecular beam epitaxy (MBE) techniques, we grew $Mn_2CoAl_{1-x}Si_x$ epitaxial films up to $x = 0.3$. For $x = 0.225$, a very small σ_{AHC} of ~ 1.1 S/cm was obtained and the sign reversal of σ_{AHC} was seen at around $x = 0.25$. We considered that one of the origins of the sign reversal of σ_{AHC} is the shift of the position of the Fermi level in the experimentally obtained MCA. However, the large number of carrier (hole) concentrations of $\sim 10^{22}$ cm^{-3} could not be suppressed in the films, meaning that the SGS-like electronic band structure is broken. From now on, we should suppress the disorder such as antisite defects to achieve a realistic SGS electronic band structure even in the film samples.

ACKNOWLEDGMENT

This work was partly supported by a Grant-in-Aid for Scientific Research (A) (Grant No. 16H02333) from the Japan Society for the Promotion of Science (JSPS).

[1] X. L. Wang, Phys. Rev. Lett. **100**, 156404 (2008).
[2] X. L. Wang, S. X. Dou, and C. Zhang, NPG Asia Mater. **2**, 31 (2010).
[3] X. Wang, Z. Cheng, J. Wang, X. L. Wang, and G. Liu, J. Mater. Chem. C **4**, 7176 (2016).
[4] H. Ohno, Science **281**, 951 (1998).
[5] S. Ouardi, G. H. Fecher, C. Felser, and J. Kübler, Phys. Rev. Lett. **110**, 100401 (2013).
[6] S. Skaftouros, K. Özdogan, E. Sasioglu, and I. Galanakis, Appl. Phys. Lett. **102**, 022402 (2013).
[7] G. Z. Xu, E. K. Liu, Y. Du, G. J. Li, G. D. Liu, W. H. Wang, and G. H. Wu, Europhys. Lett. **102**, 17007 (2013).
[8] G. Y. Gao and K.-L. Yao, Appl. Phys. Lett. **103**, 232409 (2013).
[9] I. Galanakis, K. Özdogan, E. Sasioglu, and S. Blügel, J. Appl. Phys. **115**, 093908 (2014).
[10] A. Jakobsson, P. Mavropoulos, E. Sasioglu, S. Blügel, M. Lezaic, B. Sanyal, and I. Galanakis, Phys. Rev. B **91**, 174439 (2015).
[11] L. Bainsla and K. G. Suresh, Appl. Phys. Rev. **3**, 031101 (2016).
[12] M. E. Jamer, B. A. Assaf, T. Devakul, and D. Heiman, Appl. Phys. Lett. **103**, 142403 (2013).
[13] M. E. Jamer, B. A. Assaf, G. E. Sterbinsky, D. A. Arena, and D. Heiman, J. Appl. Phys. **116**, 213914 (2014).
[14] G. Z. Xu, Y. Du, X. M. Zhang, H. G. Zhang, E. K. Liu, W. H. Wang, and G. H. Wu, Appl. Phys. Lett. **104**, 242408 (2014).
[15] N. Y. Sun, Y. Q. Zhang, H. R. Fu, W. R. Che, C. Y. You, and R. Shan, AIP Adv. **6**, 015006 (2016).
[16] K. Ueda, S. Hirose, and H. Asano, Appl. Phys. Lett. **110**, 202405 (2017).
[17] D. Bombor, C. G. F. Blum, O. Volkonskiy, S. Rodan, S. Wurmehl, C. Hess, and B. Büchner, Phys. Rev. Lett. **110**, 066601 (2013).
[18] E. V. Vidal, G. Stryganyuk, H. Schneider, C. Felser, and G. Jakob, Appl. Phys. Lett. **99**, 132509 (2011).
[19] J. Kudrnovský, V. Drchal, and I. Turek, Phys. Rev. B **88**, 014422 (2013).
[20] H. Akai, J. Phys. Soc. Jpn. **51**, 468 (1982).
[21] J. Korringa, Physica **13**, 392 (1947).
[22] W. Kohn and N. Rostoker, Phys. Rev. **94**, 1111 (1954).
[23] J. P. Perdew, K. Burke, and M. Ernzerhof, Phys. Rev. Lett. **77**, 3865 (1996).
[24] H. Shiba, Prog. Theor. Phys. **46**, 77 (1971).
[25] P. Soven, Phys. Rev. B **2**, 4715 (1970).
[26] K. Hamaya, H. Itoh, O. Nakatsuka, K. Ueda, K. Yamamoto, M. Itakura, T. Taniyama, T. Ono, and M. Miyao, Phys. Rev. Lett. **102**, 137204 (2009).

[27] S. Yamada, K. Tanikawa, S. Oki, M. Kawano, M. Miyao, and K. Hamaya, Appl. Phys. Lett. **105**, 071601 (2014).
[28] Y. Fujita, M. Yamada, M. Tsukahara, T. Oka, S. Yamada, T. Kanashima, K. Sawano, and K. Hamaya, Phys. Rev. Appl. **8**, 014007 (2017).
[29] H. Luo, Z. Zhu, L. Ma, S. Xu, X. Zhu, C. Jiang, H. Xu, and G. Wu, J. Phys. D: Appl. Phys. **41**, 055010 (2008).
[30] Y. Xin, H. Hao, Y. Ma, H. Luo, F. Meng, H. Liu, E. Liu, and G. Wu, Intermetallics **80**, 10 (2017).
[31] N. Nagaosa, J. Sinova, S. Onoda, A. H. MacDonald, and N. P. Ong, Rev. Mod. Phys. **82**, 1539 (2010).
[32] P. Giannozzi *et al.*, J. Phys.: Condens. Matter. **21**, 395502 (2009).
[33] N. Marzari and D. Vanderbilt, Phys. Rev. B **56**, 12847 (1997).
[34] G. D. Liu, X. F. Dai, H. Y. Liu, J. L. Chen, Y. X. Li, G. Xiao, and G. H. Wu, Phys. Rev. B **77**, 014424 (2008).
[35] Y. Yao, L. Kleinman, A. H. MacDonald, J. Sinova, T. Jungwirth, D.-S. Wang, E. Wang, and Q. Niu, Phys. Rev. Lett. **92**, 037204 (2004).
[36] J. Kübler and C. Felser, Phys. Rev. B **85**, 012405 (2012).
[37] X. Wang, J. R. Yates, I. Souza, and D. Vanderbilt, Phys. Rev. B **74**, 195118 (2006).
[38] A. A. Abrikosov, Phys. Rev. B **58**, 2788 (1998).